

Spatial patterns and driving mechanisms of mid-Holocene hydroclimate in western North America

NICHOLAS WAYNE HERMANN,¹ JESSICA LEIGH OSTER^{1*} and DANIEL ENRIQUE IBARRA²

¹Department of Earth and Environmental Sciences, Vanderbilt University, Nashville, TN, USA

²Department of Earth System Science, Stanford University, Stanford, CA, USA

Received 16 March 2017; Revised 5 January 2018; Accepted 22 January 2018

ABSTRACT: Mid-Holocene paleoclimate proxy records from drought-sensitive western North America suggest widespread aridity in areas dominated by winter precipitation. We present spatial comparisons of a diverse network of moisture-sensitive proxies with 12 global circulation model simulations from the Paleoclimate Model Intercomparison Project to determine the most important atmospheric drivers behind observed mid-Holocene aridity in this region. Although model-proxy agreement is low for most models, in part reflecting small mid-Holocene precipitation anomalies, three show relatively strong agreement by successfully simulating arid conditions across the Pacific Northwest. The model that shows the strongest spatial agreement with the proxy network reveals an anticyclonic wind anomaly that is similar to but weaker than anomalies noted during west-wide drought episodes of the past 500 years. This model suggests increased transient upper level ridging that reduced winter water vapor transport from the south-west during the mid-Holocene. These mechanisms are similar to those suggested to have supported megadrought conditions in western North America during the Medieval Climate Anomaly and which are also simulated in anthropogenic warming scenarios. Future work on quantitative proxy records to enhance temporal and spatial coverage, and explicitly address issues of seasonality, will improve the quality of future climate model–data comparison studies. Copyright © 2018 John Wiley & Sons, Ltd.

KEYWORDS: Cohen's kappa; mid-Holocene; proxy–model comparison; terrestrial hydroclimate; western North America.

Introduction

Terrestrial paleoclimate proxy records provide windows into past periods of drought and reveal the spatiotemporal patterns of regional effective moisture deficits. Comparison of proxy records to paleoclimate model simulations (e.g. Thompson *et al.*, 1993; Harrison *et al.*, 2003; DiNezio and Tierney, 2013; Oster *et al.*, 2015) can assist in determining the driving mechanisms behind past droughts, thereby improving our understanding of present droughts and our ability to predict future ones (Harrison *et al.*, 2015). Such comparisons are critical in furthering our understanding of mid-latitude circulation, storm track dynamics and Northern Hemisphere atmospheric circulation (Bony *et al.*, 2015; Horton *et al.*, 2015).

Western North America provides a unique case study for model–proxy comparison, as more than a century of research has resulted in what is perhaps the densest and most diverse coverage of paleoclimate proxy records available in the mid-latitudes. Pioneering model–proxy comparison work in the 1980s (COHMAP Members, 1988) and 1990s (Thompson *et al.*, 1993; Bartlein *et al.*, 1998) revealed regional patterns of hydroclimatic changes from the Last Glacial Maximum to the present and suggested forcing mechanisms behind these changes. Proxy compilations have suggested that western North America, a region sensitive to hydroclimate variability, was characterized by widespread aridity and potentially multi-decadal to centuries-long ‘mega-droughts’ during the early and middle Holocene (~9–5 ka) (Thompson *et al.*, 1993). Increased aridity was especially prominent in the Pacific Northwest in the early Holocene near 9 ka when the seasonal insolation contrast was at its highest. This aridity has been attributed to an intensified Pacific sub-tropical

high-pressure system that led to warm, stable and dry air over the region exacerbated by enhanced evaporation due to greater summer insolation (Thompson *et al.*, 1993; Gavin and Brubaker, 2015). In contrast, wetter conditions prevailed in the south-west region due to both establishment of the monsoon by ~9 ka and higher than modern levels of winter precipitation that lingered due to the waning influence of the retreating Laurentide Ice Sheet, which may have altered the path of the winter storm track in this region (Metcalf *et al.*, 2015).

Among paleoclimate records from the Pacific Northwest, many suggest a long-term trend of increasing wetness beginning in the mid-Holocene around 6 ka until present (e.g. Shuman and Serravezza, 2017) as the seasonal insolation contrast decreased. Thus, in many northern records, hydroclimatic anomalies recording dry conditions are diminished at 6 ka relative to 9 ka (Thompson *et al.*, 1993; Gavin and Brubaker, 2015). In the south-west, proxies suggest North American Monsoon strength peaked around 6 ka, while winter precipitation declined (Metcalf *et al.*, 2015). Thus, the mid-Holocene represents a time of enhanced aridity that occurred during the transition to modern boundary conditions from conditions characterized by increased seasonal insolation contrast and a declining ice sheet in the early Holocene.

We examine the spatial expression of hydroclimate in western North America during this transitional mid-Holocene interval. We combine recently published records with foundational proxy record compilations from this region (e.g. Thompson *et al.*, 1993; Harrison *et al.*, 2003) as well as more recent sub-regionally focused compilations (e.g. Metcalf *et al.*, 2015; Gavin and Brubaker, 2015). We then compare this network of proxy records with simulated annual precipitation and effective moisture from 12 mid-Holocene (6 ka) GCM simulations (Braconnot *et al.*, 2012) conducted as part of the Paleoclimate Model Intercomparison Project (PMIP3)

*Correspondence: Jessica Leigh Oster, as above.
E-mail: jessica.l.oster@vanderbilt.edu

to conduct a systematic spatial analysis of the patterns and controls on precipitation variability in this region during this transitional time.

Previous model–proxy comparisons of the 6 ka time slice have suggested that, while models successfully reproduce the sign of temperature patterns during the mid-Holocene, they have difficulty predicting the precipitation changes recorded by geologic proxies in western North America (Diffenbaugh and Sloan, 2004; Harrison *et al.*, 2014). However, these previous comparisons have focused on global rather than regional model–proxy agreement (Harrison *et al.*, 2014), used qualitative rather than quantitative comparisons (Thompson *et al.*, 1993; Mock and Brunelle-Daines, 1999; Diffenbaugh and Sloan, 2004), drawn climate information only from a single proxy type (Harrison *et al.*, 2014, 2016), or used too few paleoclimate records to sufficiently characterize the western US (Diffenbaugh and Sloan, 2004; Harrison *et al.*, 2014). Thus, it is not clear from existing comparisons why model–proxy disagreement arises and to what degree they are driven by model inaccuracies or insufficient characterization of past climate by proxies in this topographically complex, mid-latitude region.

We conduct our comparison using a weighted Cohen's Kappa (κ_w) statistic (Cohen, 1968) to quantitatively assess agreement between model output and proxy records. Cohen's Kappa measures categorical data agreement between two raters who classify items (here, proxy locations) into categories (wetter, drier or no change relative to modern) relative to the probability of random agreement. This approach has provided a useful basis for evaluating the relative importance of the drivers behind past climate and environmental changes by identifying the models that most closely match the paleoclimate record for further investigation into atmospheric dynamics (e.g. DiNezio and Tierney, 2013; Oster *et al.*, 2015; Chevalier *et al.*, 2017), and by determining agreement among different vegetation model simulations (e.g. Diffenbaugh *et al.*, 2003). This approach, applied to the mid-Holocene, can determine which models most closely match the pattern of hydroclimatic change suggested by the rich network of proxies in western North America and provide insight into the driving mechanisms behind increased aridity and larger scale circulation changes.

Methods

We compiled a network of 170 published moisture-sensitive proxy records from western North America that cover the mid-Holocene. The network includes proxies from lake sediments, packrat middens, speleothems, submerged tree stumps, pollen records and mammal fossils (Supporting Information, Table S1). To compile this network, we drew on previously published regional compilations, including Thompson *et al.* (1993) for all of western North America, Metcalfe *et al.* (2015) for the south-west, and Gavin and Brubaker (2015) for the Pacific Northwest. Records included in these previous compilations account for 93 of the 170 records in this network, the rest being records we independently extracted from the literature. We categorized each proxy site as recording drier (D) conditions, wetter (W) conditions or unchanged conditions (NC) relative to present-day conditions, reflecting the original authors' interpretations of hydroclimatic change for the period 6.0 ± 1.0 ka (Fig. 1a). This time window for the mid-Holocene (6.0 ± 1.0 ka) follows the convention put forward by Thompson *et al.* (1993). We traced records in previous compilations back to their original references to verify the moisture designation. We treat this time window as a snapshot relative to modern conditions. For

example, in many Pacific Northwest records, conditions at 6 ka reflect a trend of increasing wetness to the present, which we designate as drier than modern conditions. Records for which a distinct seasonality of hydroclimate response is suggested by the authors are noted in Table S1. For example, a proxy that suggests wetter summer conditions may be designated as 'wetter'. However, care was taken to determine the overall or dominant moisture designation on a case by case basis, and seasonality of the record is noted. As seasonality of response cannot be determined in most records, we determined that the most straightforward and consistent approach is to compare the proxy designations to annually averaged model output for the purposes of calculating κ_w (see below). However, seasonal changes in precipitation are discussed with qualitative comparisons to the proxy network. In some instances, records that had been designated as wetter, drier or unchanged in the Thompson *et al.* (1993) compilation have been listed as 'inconclusive' in our network due to poorly resolved chronologies. In our proxy network, 91 sites are identified as drier during the mid-Holocene, 27 are identified as wetter, 29 exhibit no change in moisture conditions relative to the present, and 23 are determined to be inconclusive (Fig. 1a).

Spatial coverage of proxy records is uneven across the region, with areas of highest density coverage in southern California, and the Pacific Northwest. To reduce over-representation of densely studied areas, we followed a procedure similar to DiNezio and Tierney (2013). We use ArcGIS 10.2 (ESRI, 2014) to outline a 25-km buffer radius around each site and then combined overlapping proxy sites. We selected this radius to be significantly shorter than the spatial scale of precipitation coherence in the western United States (Parker and Abatzoglou, 2016) so as not to oversimplify variability in hydroclimate response arising due to topography. This resulted in the grouping of 82 of our original sites into 32 aggregate sites, listed in Table S2. In 69% of instances (22/32), all the sites or a clear majority of sites in an aggregate group had the same moisture designation, and this was used as the designation for the new aggregate site. If a group consisted of an even split of drier and wetter sites (3/32), the aggregate site was classified as no change (NC). If a group consisted of an even split between sites suggesting unchanged conditions and sites suggesting either drier or wetter conditions (7/32), the aggregate site was classified using the site designation that exhibited change (either drier or wetter). Aggregate site coordinates were taken to be the centroid of the overlapping proxy site radii. This condensed proxy network, which also has inconclusive sites removed, consists of 97 sites with 66 classified as drier, 14 classified as no change and 17 classified as wetter relative to modern conditions (Fig. 1B; Tables S2 and S3).

We compared this proxy network with the output of monthly climatologies from 12 PMIP3 climate models of mid-Holocene (6 ka) climate accessed through the CMIP5 data portal Earth System Grid Federation (ESGF) (Taylor *et al.*, 2012). Simulation of terrestrial hydroclimate in global climate models can differ between models due to differences in model resolution, land-surface models of water partitioning, albedo representations and energy budget schemes, as well as complexity in cloud microphysics controlling precipitation rates, large-scale circulation patterns and orographic precipitation (e.g. Delire *et al.*, 2002; Dai, 2006; Trenberth, 2011; Dalmonech *et al.*, 2015). We used bilinear interpolation to calculate precipitation and effective moisture (EM) values from average monthly precipitation (P) and evapotranspiration (E) of the 6 ka and Pre-Industrial (0 ka) runs from the 12 models in their native resolution (Table 1) using coordinates

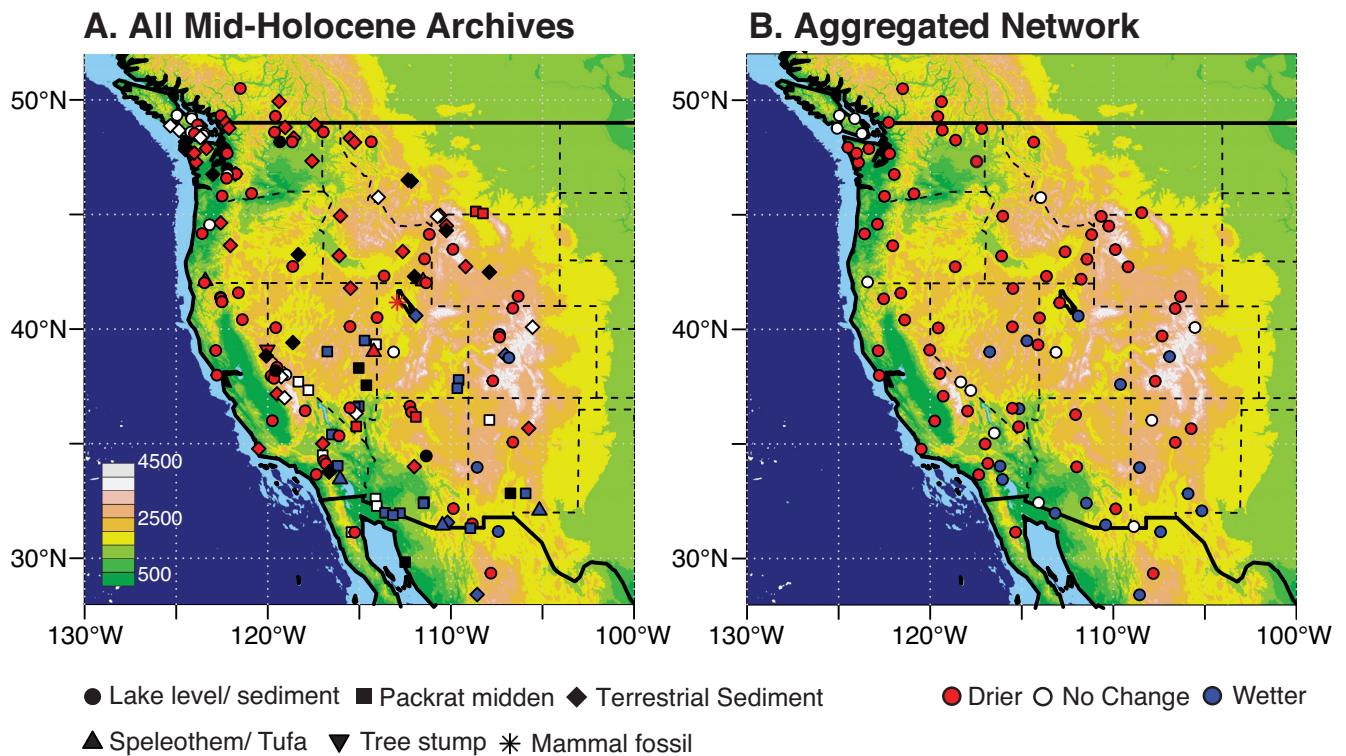


Figure 1. (A) Mid-Holocene proxy network from western North America designated by the type of archive (symbol) and the hydroclimate designation relative to modern (color). See Table S1 for a complete list of record locations and references. (B) Aggregated proxy network used in κ_w calculation. Underlying map shows topographic relief (m) of western North America generated using ETOPO1 (NOAA, 2008).

of the proxy sites or centroids of the search radius for aggregate sites. EM was calculated following Equation (1). Next, we calculated annual precipitation and EM anomalies between the 6 ka and 0 ka simulations using Equations (2) and (3):

$$EM = P - E \quad (1)$$

$$P_{Anom} = (P_{6ka}/P_{0ka}) \times 100 \quad (2)$$

$$EM_{Anom} = (EM_{6ka}/EM_{0ka}) \times 100 \quad (3)$$

Anomalies are thus expressed as per cent changes in average annual precipitation taken from the monthly climatology output relative to the 0 ka Pre-Industrial run for each model.

We compare the hydroclimatic changes simulated by each model with the change observed in each proxy record by using a weighted Cohen's κ_w statistic (e.g. DiNezio and Tierney, 2013; Oster *et al.*, 2015), which weights observations according to the degree of model-proxy disagreements (Cohen, 1968). This is accomplished by multiplying a matrix of model-proxy observations by a weight matrix in which strong agreement between observers (e.g. both the model and

Table 1. Climate model descriptions.

Model name	Model ID	Number of grid cells (lat.)	Number of grid cells (long.)	Resolution (° lat.)	Resolution (° long.)	Mid-Holocene simulation length (years)	Pre-Industrial simulation length (years)	Institution
BCC-CSM1-1	BCC	64	128	2.81	2.81	100	500	BCC, China
CCSM4	CCSM4	192	288	0.94	1.25	301	156	NCAR, USA
CNRM-CM5	CNRM	128	256	1.41	1.41	200	850	CNRM-CERFACS, France
CSIRO-MK3-6-0	CSIRO 360	96	192	1.88	1.88	100	500	CSIRO-OCCE, Australia
CSIRO-MK3L-1-2	CSIRO 312	56	64	3.21	5.63	500	1000	CSIRO-OCCE, Australia
FGOALS-g2	FGOALS-g2	60	128	2.81	2.81	686	900	LASG-CES, China
FGOALS-s2	FGOALS-s2	108	128	1.66	2.81	100	501	LASG-IAP, China
GISS-E2-R	GISS	90	144	2.00	2.50	100	1200	NASA-GISS, USA
IPSL-CM5A-LR	IPSL	96	96	1.88	3.75	500	1000	IPSL, France
MIROC-ESM	MIROC	64	128	2.81	2.81	100	630	MIROC, Japan
MPI-ESM-P	MPI	96	192	1.88	1.88	100	1156	MPI-M, Germany
MRI-CGCM3	MRI	160	320	1.13	1.13	101	500	MRI, Japan

the proxy suggest wetter conditions at a given site) is given a weight of 0, strong disagreement (e.g. the model suggests wetter, but the proxy suggests drier) is given a weight of one and weak disagreement (e.g. the model suggests wetter, but the proxy suggests no change) is given a weight of 0.5. κ_w is then calculated as:

$$K_W = 1 - \frac{\sum_{i=1}^C \sum_{j=1}^C w_{ij} x_{ij}}{\sum_{i=1}^C \sum_{j=1}^C w_{ij} m_{ij}} \quad (4)$$

where w_{ij} and x_{ij} are elements in the weight and observed matrices and m_{ij} are elements in the matrix of scores that would arise through random chance. To identify the maximum possible agreement between models and proxies, we varied the threshold of change in P and EM required for the model responses to fall into the wetter or drier category from 2 to 30% and calculated 95% confidence limits for the maximum κ_w for each model (Cohen, 1968). For example, at a threshold of 10%, a model must simulate mid-Holocene precipitation $\geq 110\%$ of modern for a site to be classified as wetter and $\leq 90\%$ of modern to be classified as drier. Values within this range are classified as 'no change or (NC)'. Computed κ_w values can range from -1 to 1 , where -1 is perfect disagreement, 0 is no agreement greater than random chance, and 1 is perfect agreement between the model and proxy records (Cohen, 1968). For the EM κ_w calculations, sites falling in grid cells that contain some proportion of ocean were excluded. The number of sites excluded from the calculation for EM varied from model to model due to differing model resolution (Table 2). This number ranged from three to 13 sites being removed from the EM calculation.

In general, the models simulate small precipitation and EM anomalies for the mid-Holocene, and so we also explored the model-proxy agreement more closely by applying a two-sided Kolmogorov–Smirnov (KS) test (Massey, 1951) to the model output to determine the distribution of significantly wetter and drier mid-Holocene conditions. To do this, we used the entire monthly model precipitation and evaporation output for all model years following initialization and spin-up in the 6 ka and 0 ka model runs, rather than the monthly climatology (average monthly) output used in the previous test. The KS test method compares the distance between the cumulative distribution functions of precipitation and EM simulated for the mid-Holocene and pre-industrial distributions. By comparing the distance between the cumulative distribution functions each proxy location is determined to be drier, wetter, or unchanged during the mid-Holocene relative to the pre-industrial at a 95% confidence level. Following this classification, we then calculate κ_w values for each model comparing the KS test categorization and proxy network classifications. We were able to perform this analysis on the seven models that archived monthly output (Table 2).

To analyze atmospheric pressure patterns within each model, we identified model grid cells with maximum and minimum pressures over the Pacific Ocean to locate pressure centers of the North Pacific High (NPH) and Aleutian Low (AL), respectively (Caballero and Hanley, 2012; Oster *et al.*, 2015) for both annually and seasonally averaged (winter and summer) model output. We used multiple linear regression analysis using an Akaike information criterion (Burnham and Anderson, 2002) to determine which pressure configurations (latitude, longitude, sea level pressure, and pressure difference between the high and low) correlated with model agreement with the proxy network (κ_w) using the MuMIn

package in R (Bartoń, 2014) testing both annual and seasonally averaged values.

Results and discussion

Observed mid-Holocene proxy network

Today, western North America exhibits a seasonal precipitation gradient in which the influence of winter storms derived from the westerly storm track declines from west to east (Fig. 2, top panel) as the influence of the North American Monsoon and moisture from the Gulf of Mexico and Gulf of California increases (Adams and Comrie, 1997; Higgins and Shi, 2005; Mejia *et al.*, 2016). The observed mid-Holocene moisture pattern provides evidence of consistently drier conditions in the region dominated by winter westerly storm-derived precipitation. Areas in the south-west with potential monsoonal influence show a mixed response (Fig. 1). The Pacific Northwest, northern Rockies and most of California were exclusively drier or similar to modern, while sites in the Great Basin and southern Rockies indicate a mixture of wetter, drier and similar conditions at 6 ka relative to present. A majority of proxies, especially at the US–Mexico border, suggest the desert south-west was wetter at 6 ka, although Colorado Plateau sites in northern Arizona and New Mexico were drier than modern. The pattern of hydroclimatic change exhibited in our updated proxy network is spatially similar to that presented by Thompson *et al.* (1993). Proxy coverage has improved in California, Oregon and the Rocky Mountains, and the subtleties in regional variations are more apparent in the new compilation. For example, enhanced aridity in all but the southernmost portion of California is evident in our new compilation, while much of the state is designated as 'no change' in the Thompson *et al.* (1993) compilation. Likewise, records in this new compilation suggest increased aridity in northern Arizona and New Mexico and more variability among proxies in the Colorado Rockies than was apparent in the compilation of Thompson *et al.* (1993). Similar variability in hydroclimate response is observed across the southern Great Basin in both compilations. In the Pacific Northwest, Thompson *et al.* (1993) and Thompson and Anderson (2000) observe inland aridity coupled with near-modern conditions along the coast. In our compilation, the near-modern or unchanged conditions are largely restricted to Vancouver Island, with drier conditions extending to the coast farther south. Our proxy compilation is also consistent with previous studies that suggested an enhanced North American monsoon during the mid-Holocene (Mock and Brunelle-Daines, 1999; Metcalfe *et al.*, 2015), in particular along the US–Mexico border, as proxy records suggest wetter conditions in that region.

Model-proxy comparison

On the whole, models included in the PMIP3/CMIP5 ensemble reproduce broad-scale precipitation patterns outside of the tropics when compared with modern observations (IPCC AR5) including patterns of precipitation anomalies associated with the El Niño/Southern Oscillation (ENSO) for North America (Fuentes-Franco *et al.*, 2016). Further, CMIP5 model accuracy for modern total precipitation and seasonality is highest, and shows the least spread among ensemble members, in mid-latitude regions such as western North America (Koutroulis *et al.*, 2016). We found that the models included in our comparison were able to qualitatively reproduce seasonal precipitation patterns in western North America, and also that they did not simulate a significant change in the

Table 2. κ_w results and proxy site agreement.

Model	Precipitation			Effective moisture			Sites removed from EM calculation
	Max. κ_w^*	Threshold (%)	KS $\kappa_w^{*\dagger}$	Max. κ_w^*	Threshold (%)	KS $\kappa_w^{*\dagger}$	
FGOALS-g2	0.300	2	0.276	0.346	2	0.273	3
MPI	0.295	2	0.199	0.386	2	0.130	4
IPSL	0.205	4	0.150	0.395	2	0.298	9
CSIRO 312	0.148	10	−0.006	0.099	40	−0.071	10
MIROC	0.168	4	0.150	0.151	6	0.032	13
CSIRO 360	0.151	10	NA	0.129	40	NA	4
MRI	0.159	2	NA	0.226	4	NA	4
FGOALS-s2	0.161	4	0.061	0.096	8	−0.018	9
CNRM	0.127	2	0.071	0.147	6	0.021	6
BCC	0.086	6	NA	0.104	8	NA	3
GISS	0.079	2	NA	0.134	6	NA	9
CCSM4	0.017	2	NA	−0.040	40	NA	7

*Values in bold are significantly greater than zero at the 95% confidence interval.

†NA is given for models that did not archive monthly precipitation output.

seasonality of precipitation between the 6 ka and Pre-Industrial model runs (Fig. 2). In general, the PMIP3/CMIP5 models have also been shown to slightly underestimate the magnitude of mid-Holocene precipitation anomalies in North America as a whole, although the simulated anomalies fall within the uncertainty of the changes estimated from paleoclimate reconstructions (Braconnot *et al.*, 2012).

Overall, agreement between the proxy network and the mid-Holocene climate simulations is low (κ_w values of 0.3 and below) for both annual precipitation and EM anomalies (Fig. 3). However, most models show higher than modern (where modern = pre-industrial) average annual precipitation (Fig. S1) and EM (Fig. S2) at the US–Mexico border during the mid-Holocene, which is consistent with most proxies from this region (Fig. 1). In contrast, all models show poor agreement with the proxy network in California and the Colorado Plateau, where proxies indicate lower than modern precipitation and EM during the mid-Holocene, and models show higher precipitation and EM (Fig. 4).

Of the 12 models, FGOALS-g2 and MPI-ESM-P (hereafter, MPI), and IPSL-CM5A-LR (hereafter, IPSL) have the highest κ_w values for precipitation and EM (Fig. 3; Table 2). In particular, these models are the only ones to show decreased precipitation and/or EM in the Pacific Northwest at 6 ka (Fig. 5A,C), where all other models show unchanged or increased precipitation and EM. For each of these models, the best agreement with the proxy network (the highest κ_w values) occur at the 2 and 4% thresholds, the lowest thresholds for defining a change in modeled precipitation or EM, probably because of the small precipitation anomalies simulated by the models for the mid-Holocene. The removal of coastal sites in the EM calculations did not appear to have a direct influence on EM κ_w values, as the models with the highest κ_w values ranged from few sites removed (FGOALS-G2 = 3) to many (IPSL = 9).

Using the KS test to determine modeled annual precipitation and EM anomalies in the mid-Holocene, we calculate κ_w values that are similar to but generally slightly lower than those calculated using the threshold method (Table 2). Maps of the KS test results are also shown for the top three models (Fig. 5B,D) and for all models analyzed (Figs S3 and S4) in the native gridded model output resolution. FGOALS-g2, MPI and IPSL continue to have the highest κ_w values, suggesting the closest match with the proxy network. FGOALS-g2 and IPSL again show closer agreement with the proxies for EM

than for precipitation, but MPI shows a closer agreement with precipitation using this method (Fig. 5B,D). The κ_w values calculated for MPI also show the largest decrease probably because a larger proportion of the study area is found to show no significant change (white grid cells on the map) in precipitation or EM following the KS approach (Fig. 5B,D). Overall, FGOALS-g2 shows the most consistently high agreement with the proxy network following both approaches for calculating κ_w . Further, the KS test method confirms what the threshold approach suggested, namely that mean modeled differences between the mid-Holocene and Pre-Industrial conditions are small. For example, in the FGOALS-g2 simulation, a grid cell in the Pacific Northwest found to show significant mid-Holocene drying displays a mean ΔP of only −3.9% and a mean ΔEM of only −4.6% (Fig. 6). The modeled moisture increase in the south-west is more pronounced, with an example grid cell displaying a mean ΔP of +16.7% and mean ΔEM of +42.1% during the mid-Holocene. This analysis suggests that, if these models are correct, the proxies across much of western North America may be recording a signal of increased aridity in response to modest decreases in precipitation and EM. However, our results are consistent with previous comparisons that suggest these models generally predict smaller mid-Holocene precipitation anomalies than the proxy records suggest over all of North America (Braconnot *et al.*, 2012).

Previous analysis of PMIP3 model simulations of mid-Holocene and Last Glacial Maximum (LGM) climates indicates that models are generally capable of capturing large-scale features of paleoclimate, such as the North American Monsoon and shifting westerlies, yet the ability of models to predict the proper magnitude of change, especially on a regional basis, is still in need of improvement (Harrison *et al.*, 2015, 2016). Regional climate model simulations of mid-Holocene EM also show disagreement with moisture-sensitive proxy records in western North America, with regional climate models indicating wetter than modern conditions over northern California and south-western Oregon and proxy records indicating drier than modern conditions (Diffenbaugh and Sloan, 2004). Likewise, our study suggests that the sign of change is poorly represented and inconsistent among the PMIP3 simulations of mid-Holocene hydroclimate in western North America, although some models perform better than others. Notably, the κ_w values for 6 ka simulations overall are lower than those for the PMIP3

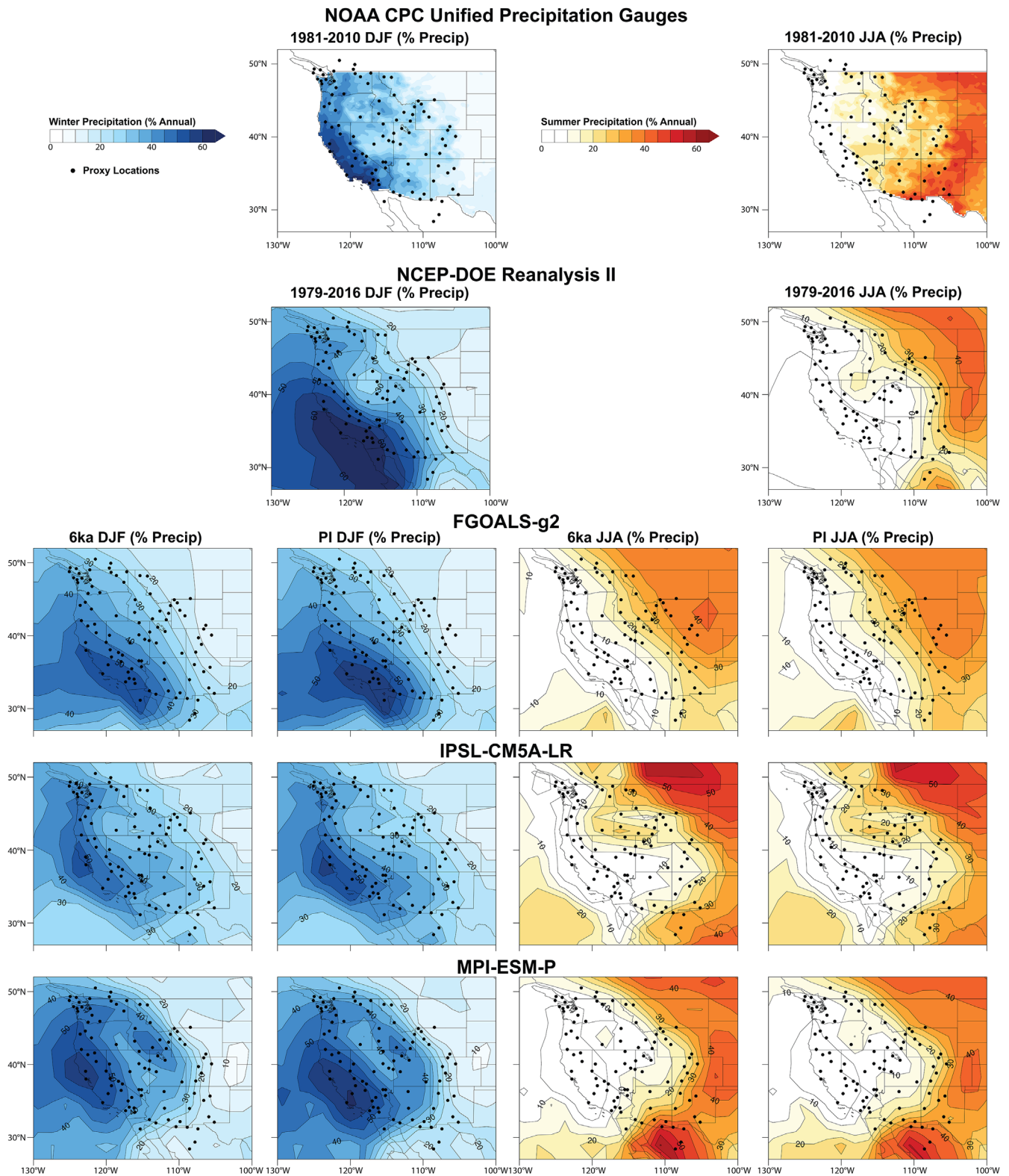


Figure 2. Per cent of annual precipitation in western North America that occurs in winter (DJF) and summer (JJA) for the present (1979–2010) calculated based on the NOAA CPC Unified precipitation gauges (top; data provided by the NOAA/OAR/ESRL PSD, Boulder, CO, US, from their website at www.esrl.noaa.gov/psd/), reanalysis data (middle) (Kanamitsu *et al.*, 2002) and then for the Pre-Industrial and mid-Holocene simulations of the top three highest scoring models in this analysis (FGOALS-g2, IPSL-CM5A-LR, MPI-ESM-P).

21 ka simulations compared to the LGM proxy network for this region (Oster *et al.*, 2015). This is probably due to the substantially smaller mean change in forcing between the mid-Holocene and Pre-Industrial control simulations, where insolation forcing is the primary variable. This results in smaller mid-Holocene precipitation and EM anomalies compared to the LGM where ice sheets and atmospheric $p\text{CO}_2$ also differ from the Pre-Industrial simulations (Braconnot *et al.*, 2012).

Driving mechanisms of mid-Holocene hydroclimate

Models showing the best agreement with the proxy network for precipitation (FGOALS-g2 and MPI-ESM-P) and EM (FGOALS-g2, IPSL and MPI) have similar mid-Holocene atmospheric configurations. Each of these three models shows positive annual westerly lower tropospheric (850 hPa) wind

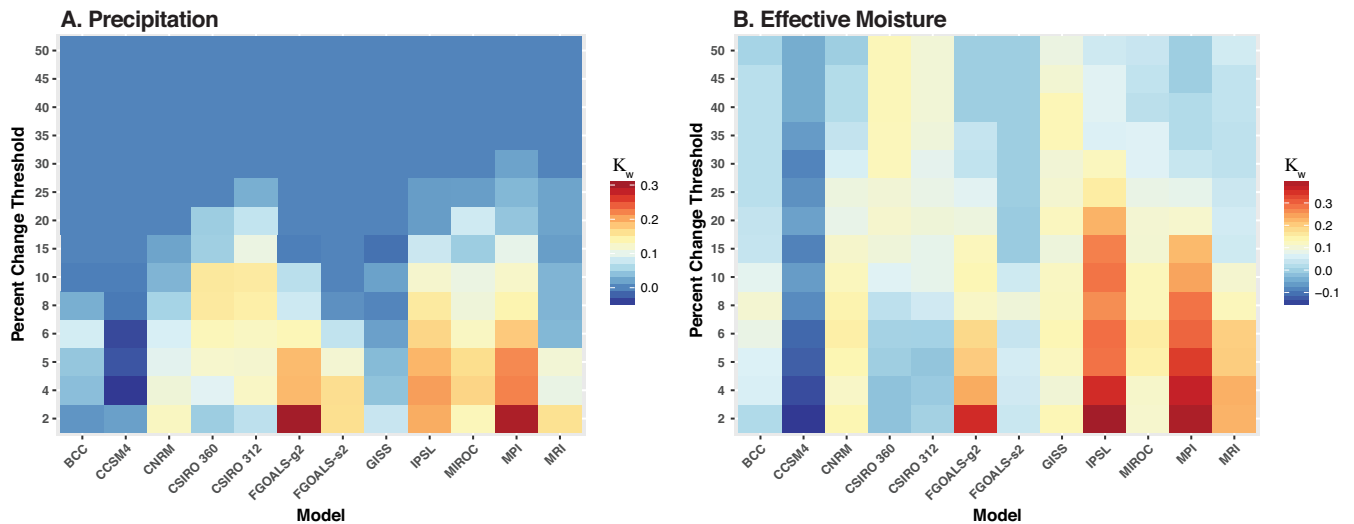


Figure 3. κ_w as a function of the percentage change threshold for (A) precipitation and (B) effective moisture for all models in this study. Maximum κ_w values are listed in Table 2.

anomalies north of 45°N in the north-east Pacific Ocean, and negative westerly lower tropospheric wind anomalies between 30 and 45°N at 6 ka, indicating a mid-Holocene climate with poleward shifted zonal winds relative to modern (Fig. 7). Multiple linear regression analysis indicates that higher model κ_w values for precipitation are correlated with a strengthened and west-shifted NPH and a weaker contrast between the NPH and AL annually ($R^2 = 0.89$, $p < 0.002$). The regression models for EM produce only slightly weaker correlations ($R^2 = 0.82$, $p < 0.002$), and also indicate that a weakened contrast between the NPH and AL plays an important role in determining agreement between modeled EM and moisture conditions as recorded by proxies in western North America. These results are consistent with the results of Thompson *et al.* (1993) which also attributed Pacific Northwest aridity to a strengthened NPH. Most of the PMIP3 models (including FGOALS-g2, IPSL and MPI) simulate only a strengthened winter NPH at 6 ka, but not a strengthened annual NPH. However, even for the best scoring models there is consistent spatial disagreement in the impact of these effects, reflected in the precipitation patterns. In particular, model-proxy agreement is quite low in California and on the southern Colorado Plateau (Fig. 4).

The mid-Holocene proxy network assembled here suggests widespread aridity throughout western North America, particularly in sites along the west coast, stretching into the northern Great Basin, Rocky Mountains and parts of the Colorado Plateau (Fig. 1). Most of these arid sites are situated in regions that are dominated by winter precipitation. The Pre-Industrial simulations of the three top models reproduce this seasonal pattern, and none of these models suggests major changes in the seasonal distribution of precipitation during the mid-Holocene (Fig. 2).

The pattern of west coast aridity expressed in the mid-Holocene proxy network is similar to so-called 'West Coast-wide dry years' noted in the last century and in the pre-instrumental tree ring record of the past 500 years (Wise, 2016). In these years, a pattern of increased aridity is evident across the west coast of North America and inland through Nevada and Idaho. FGOALS-g2 displays a similar pattern in winter precipitation anomalies during the mid-Holocene, with more pronounced aridity across all regions except the desert south-west (Fig. 8). West Coast-wide droughts over the past 500 years were often characterized by a deep

high-pressure ridge centered off the Pacific Northwest that blocked winter storms and circulated dry air into coastal regions from the continents rather than moist air from the Pacific (Wise, 2016). FGOALS-g2 simulates only weak sea-level pressure anomalies during the winter and does not exhibit the strong positive 500-hPa geopotential height anomaly that characterizes modern West Coast-wide dry years (not shown). However, the FGOALS-g2 model does simulate a similar winter anticyclonic upper atmosphere wind anomaly (250 hPa) to that seen in modern West Coast-wide droughts, confirming the existence of transient offshore upper level ridging that would have reduced moisture delivery to the continent during the mid-Holocene (Fig. 9).

FGOALS-g2 also simulates negative anomalies in integrated water vapor (IWV) over much of western North America and the Pacific during the winter. The negative IWV anomalies are stronger in the subtropical Pacific to the south-west of Western North America, suggesting less winter water vapor transport to the continent from this source region during the mid-Holocene (Fig. 9). This combination of decreased moisture transport from the south-west and stronger northerly meridional winds is consistent with other modeling studies investigating hydroclimatic variability in western North America at other times. Namely, reduced moisture transport from the south-west, possibly due to fewer atmospheric river storms, may have driven megadrought conditions in the Walker Lake Basin during the Medieval Climate Anomaly (Hatchett *et al.*, 2016). Likewise, models robustly predict drying northerly winds will influence south-western North America in global warming scenarios (Simpson *et al.*, 2016). Thus, the agreement between the FGOALS-g2 model and the mid-Holocene proxy network suggests these features are also important in establishing aridity during the mid-Holocene as well.

Precipitation patterns in western North America are also highly sensitive to ocean-atmosphere oscillations including the ENSO and the Pacific Decadal Oscillation. Hydroclimatic variability associated with these oscillations has distinct spatial fingerprints across the region at the present-day (Wise, 2010). Furthermore, recurrent megadroughts noted in this region during the Medieval Climate Anomaly appear to be associated with the cool, La Niña phase of ENSO (Seager *et al.*, 2008; Coats *et al.*, 2016). Most climate models participating in PMIP2 and PMIP3 simulate a

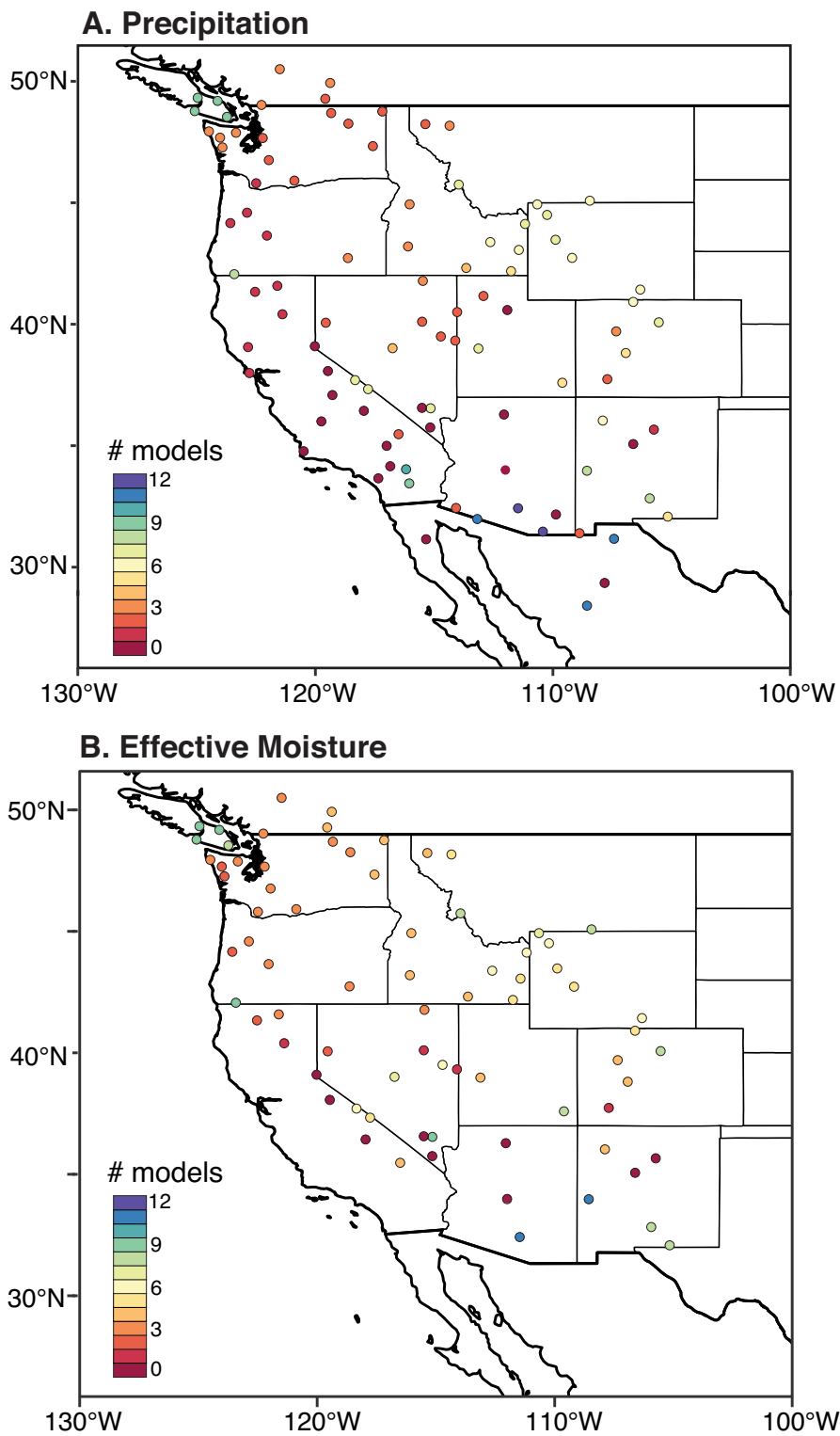


Figure 4. Proxy agreement with model ensemble for (A) mid-Holocene precipitation anomalies and (B) effective moisture (EM) anomalies. Color coding shows number of models (out of 12) in agreement with the proxy designation (wet/no change/dry) at each site. For EM, sites that fall within grid cells that contain ocean were not included in the κ_w calculations for all models depending on model resolution. These sites are not included on the EM agreement map in B.

reduction of ENSO variability during the mid-Holocene as well as a reduction in the strength of the annual cycle of the eastern equatorial Pacific (Zheng *et al.*, 2008; Karamperidou *et al.*, 2015), and these model observations have been supported by proxy records from the eastern equatorial Pacific region (e.g. Moy *et al.*, 2002; Koutavas *et al.*, 2006; Conroy *et al.*, 2008). Analysis of the CCSM4 mid-Holocene simulation has suggested that the Central Pacific (CP) and Eastern Pacific (EP) flavors of ENSO exhibited different responses to orbital forcing, with the frequency of CP events increasing and maintaining variance, while the frequency of EP events decreased with

reduced variance (Karamperidou *et al.*, 2015). An increase in CP El Niño events over EP El Niño events has also been noted for the ensemble of PMIP2 and PMIP3 6 ka simulations (An and Choi, 2014).

Teleconnections of CP and EP El Niño events to western North America display different spatial patterns of precipitation. In particular, modern observations and models suggest that a negative winter precipitation anomaly in the Pacific Northwest and a positive precipitation anomaly over the south-west is more frequently associated with CP El Niño events, while the north-west experiences a positive precipitation anomaly during EP El Niño events (Weng *et al.*, 2009;

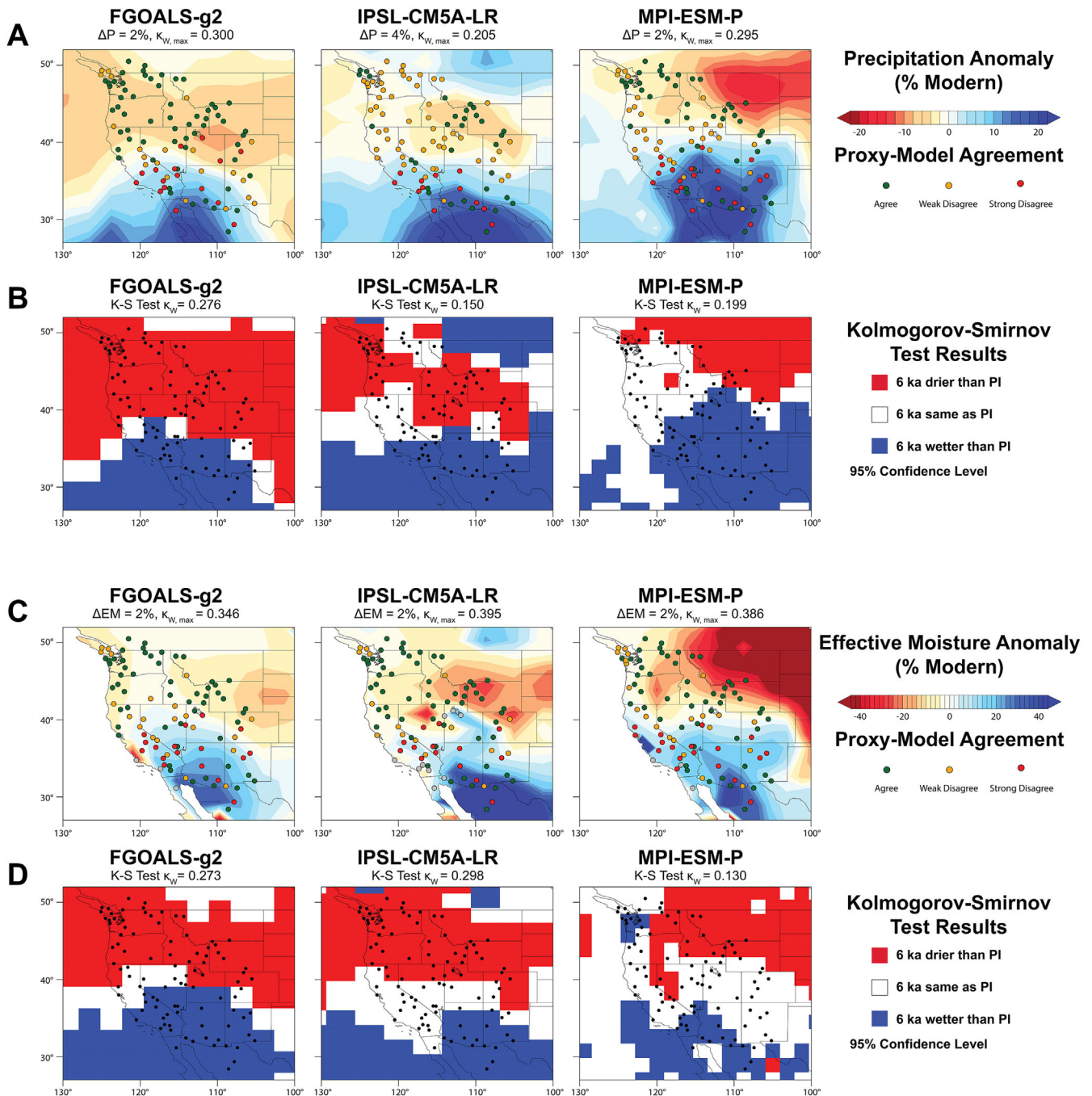


Figure 5. (A) Mean annual mid-Holocene precipitation anomalies for PMIP3 models with highest κ_W values calculated by the threshold method. Red, yellow and green dots represent proxy sites which agree, weakly disagree or strongly disagree with the modeled precipitation anomaly, respectively. (B) Wetter and drier regions at the 95% confidence interval in the same models and resulting κ_W values calculated using the KS test on modeled precipitation. (C,D) As in A and B but for effective moisture (EM).

Garfinkel *et al.*, 2013). This dry north–wet south pattern is consistent with most proxy observations for the mid-Holocene of western North America (Fig. 1), and fits with the precipitation and EM anomalies simulated by FGOALS-g2 for the mid-Holocene for annual and winter anomalies (Figs 4 and 8). This observation suggests an increase in the frequency of CP El Niño events during the mid-Holocene may explain precipitation patterns recorded by the proxy network and indicates that further investigation of this connection is warranted. Analysis of annually resolved terrestrial or offshore sediment archives (e.g. Nederbragt and Thurow, 2005), older tree rings (e.g. Griggs *et al.*, 2017) or speleothems (e.g. Myers *et al.*, 2015) from western North America may assist in determining the role of El Niño flavor in structuring hydroclimatic variability across this region during the mid-Holocene.

Challenges to proxy aggregation studies

Recent work has demonstrated the utility of aggregating the wealth of paleoclimate data that is available for western North America to investigate spatial patterns of hydroclimatic variation on multiple timescales utilizing regionally focused multi-proxy aggregates (e.g. Metcalfe *et al.*, 2015; Oster *et al.*, 2015) or proxy-specific aggregates (e.g. Oster and Kelley, 2016; Shuman and Serravezza, 2017). Efforts are now focused on globally integrating multi-proxy records, with particular interest in the last two millennia (e.g. PAGES 2k Consortium, 2013). In aggregating paleoclimate records, and in comparing proxy records to model output or to modern climate, the timescale, seasonality, and fidelity of proxy response to environmental change are important factors to

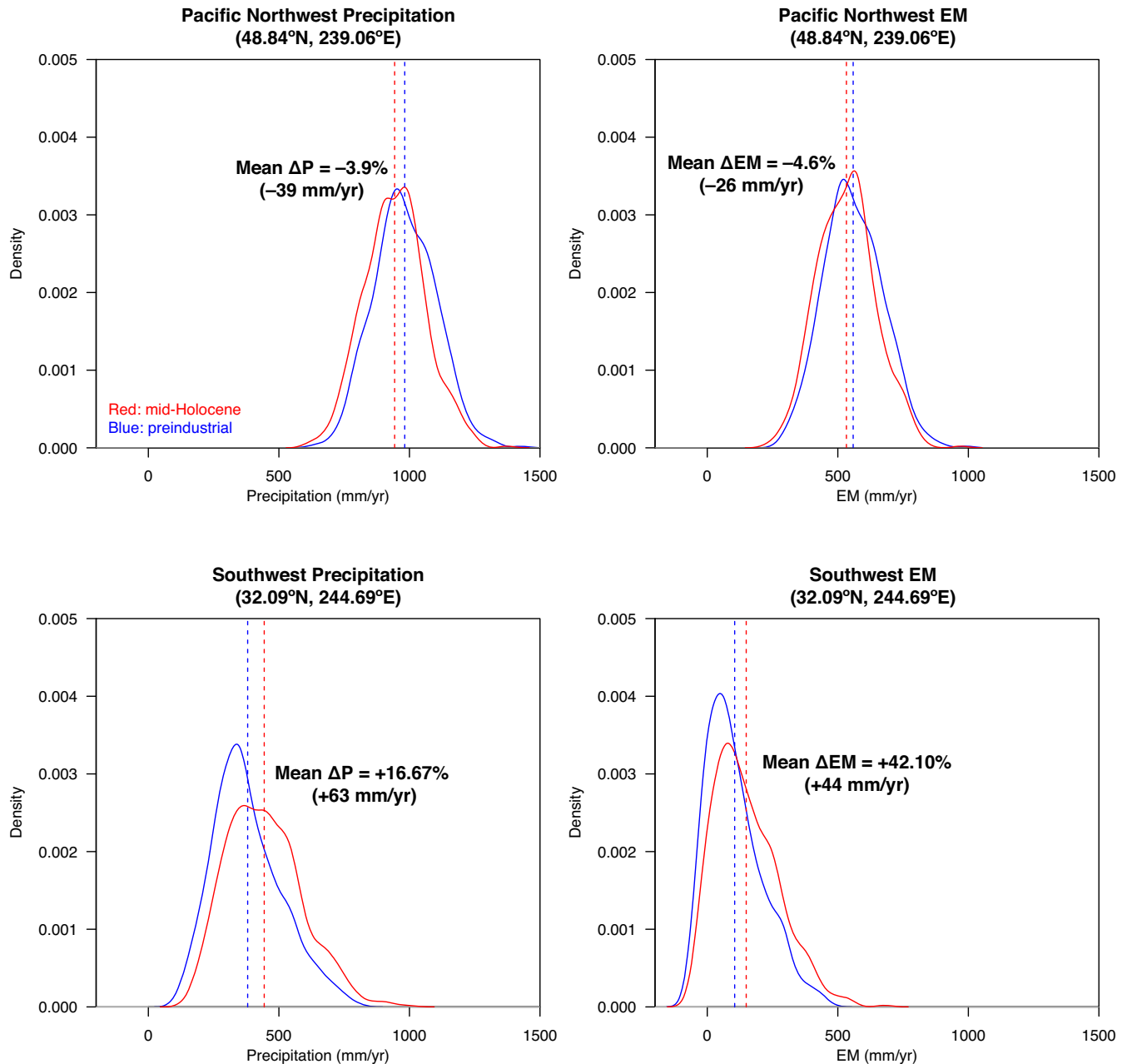


Figure 6. Probability density plots comparing mid-Holocene (red) and Pre-Industrial (blue) monthly precipitation distributions for simulations of the FGOALS-g2 model at example grid cells in the Pacific Northwest (top panels) and Southwest (bottom panels) for precipitation (left panels) and effective moisture (EM) (right panels). Dashed lines show mean precipitation and EM values for the Pre-Industrial and mid-Holocene runs, and the difference between the two is given in each panel.

consider. Our approach in this study is inclusive, recognizing that proxies record hydroclimate variability in different ways, and mitigating this variability through the inclusion of diverse proxy and archive types in our compilation (DiNezio and Tierney, 2013; Oster *et al.*, 2015). However, other strategies include extracting and compiling individual proxy types (e.g. Bartlein *et al.*, 2011; Oster and Kelley, 2016), or using only records that provide quantitative estimates of key hydroclimate variables (e.g. Lora *et al.*, 2017). Each approach has advantages as well as challenges in either sample size or consistency of the proxy responses. Moving forward, increasing the temporal and spatial coverage of proxy records that explicitly address seasonality of proxy response (Bartlein *et al.*, 2011) and provide quantitative estimates (e.g. Shuman and Serravezza, 2017) will improve the quality of climate model–data comparison studies that are possible. In western North America specifically, the generation of seasonally

specific, well-dated proxy records from regions displaying variable responses, such as the Great Basin and four-corners region (Fig. 1), may help to further elucidate driving mechanisms behind mid-Holocene hydroclimatic change.

Conclusions

Our expanded proxy compilation is consistent with prior suggestions of drier than modern conditions in the Pacific Northwest, California, northern Great Basin and northern Rocky Mountains, and wetter than modern conditions in the Desert Southwest, parts of the southern Great Basin and the Colorado Plateau. Although our model–proxy comparison is consistent with previous analyses that find low levels of agreement between the mid-Holocene proxy record and model simulations in this region, using the κ_w statistic we were able to identify three models that show the closest

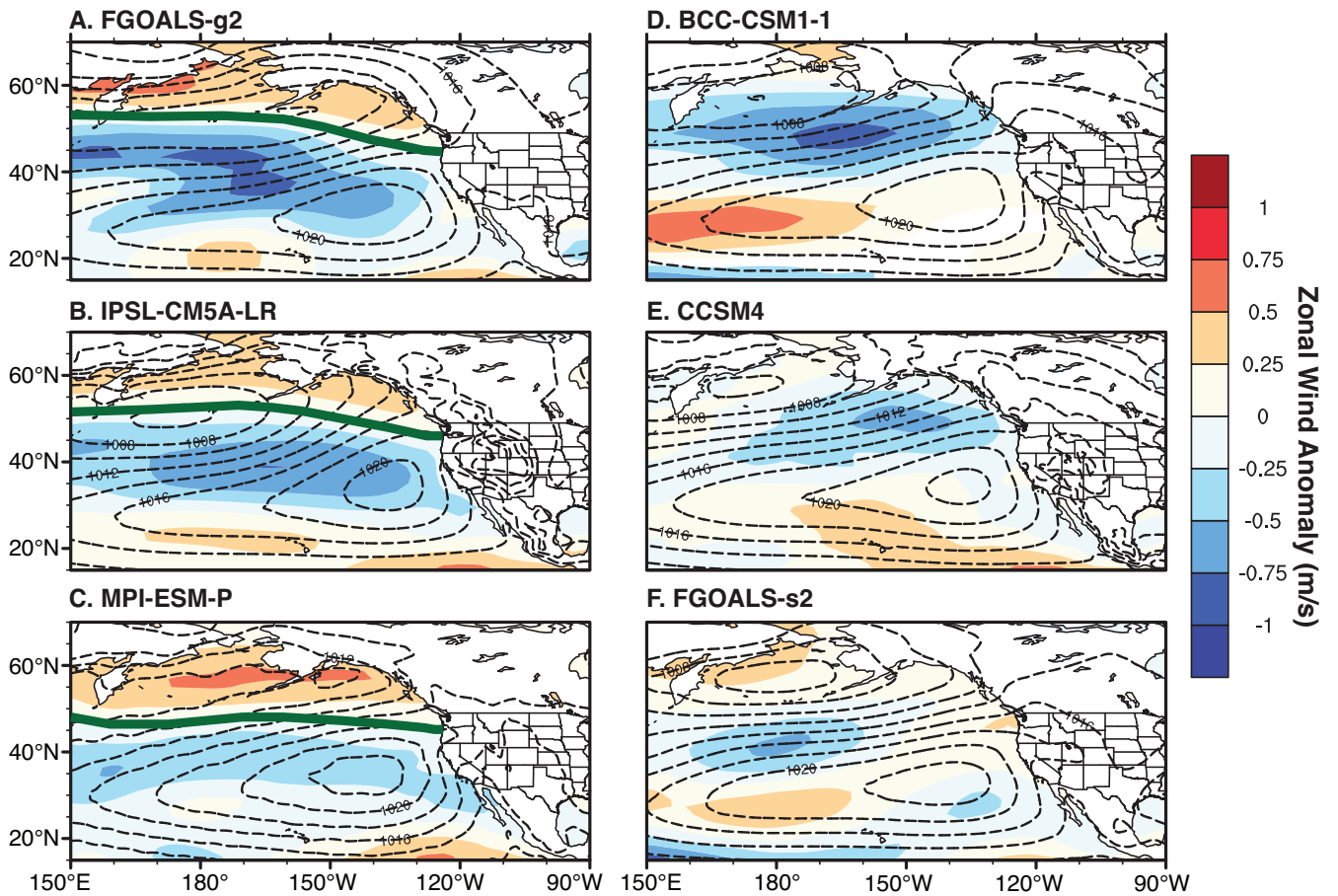


Figure 7. Annual zonal lower tropospheric (850 hPa) wind anomalies (shading) and surface pressure (dashed contours; interval = 2 hPa) for select PMIP3 models. (A–C) Models with a distinct boundary between anomalously stronger (positive) zonal winds in north of 45°N and anomalously weaker (negative) zonal winds to the south of 45°N. These models show the strongest agreement with the mid-Holocene proxy network. (D–F) Three of the nine models which do not exhibit this pattern of zonal wind anomalies and exhibit weak agreement with the proxy network.

agreement with the proxy network. Of the 12 models examined here, we find that FGOALS-g2, IPSL-CM5A-LR and MPI-ESM-P best reflect mid-Holocene precipitation and EM in western North America, with FGOALS-g2 most consistently showing closer agreement with the proxy network. In particular, these models are the only ones that capture arid conditions

in the Pacific Northwest during the mid-Holocene. Even in the models that show better agreement, the changes in precipitation simulated for the mid-Holocene are small. We find that the mechanisms driving more arid conditions in the mid-Holocene include the development of anticyclonic 250-hPa wind anomalies offshore of the Pacific Northwest including

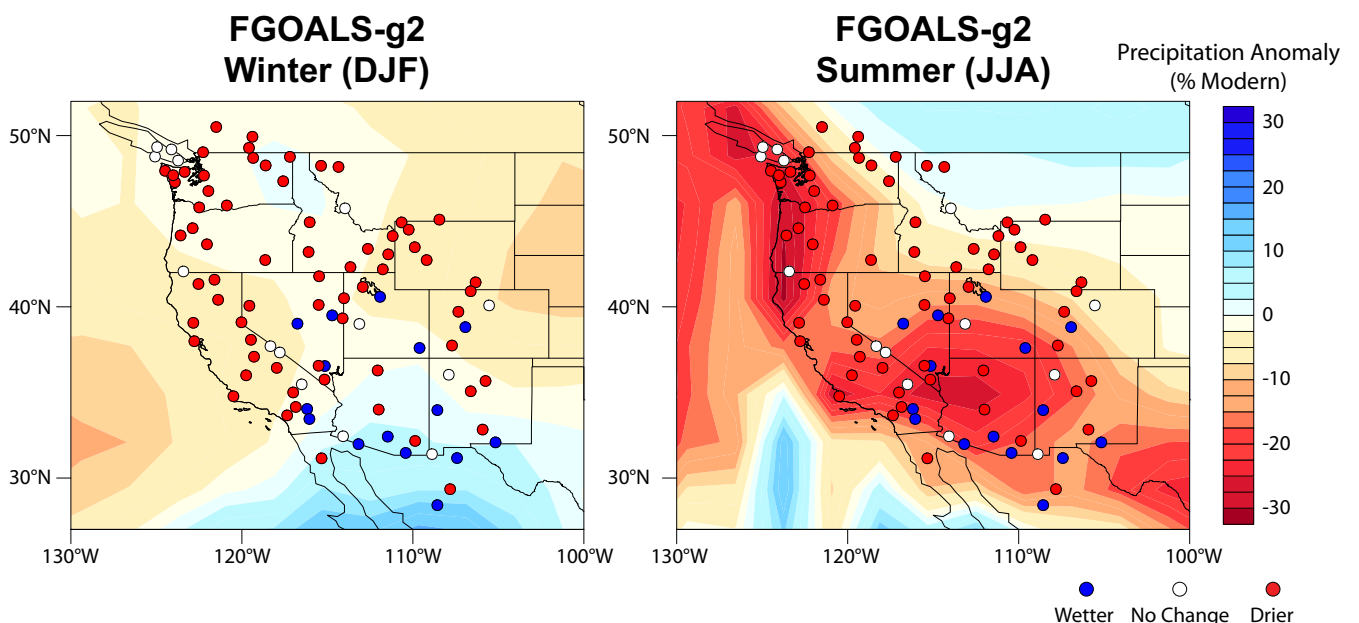


Figure 8. Winter (DJF) and summer (JJA) precipitation anomalies for the FGOALS-g2 mid-Holocene simulation (6 ka) calculated relative to the Pre-Industrial simulation (0 ka). Dots show the aggregated proxy network coded by hydroclimate designation.

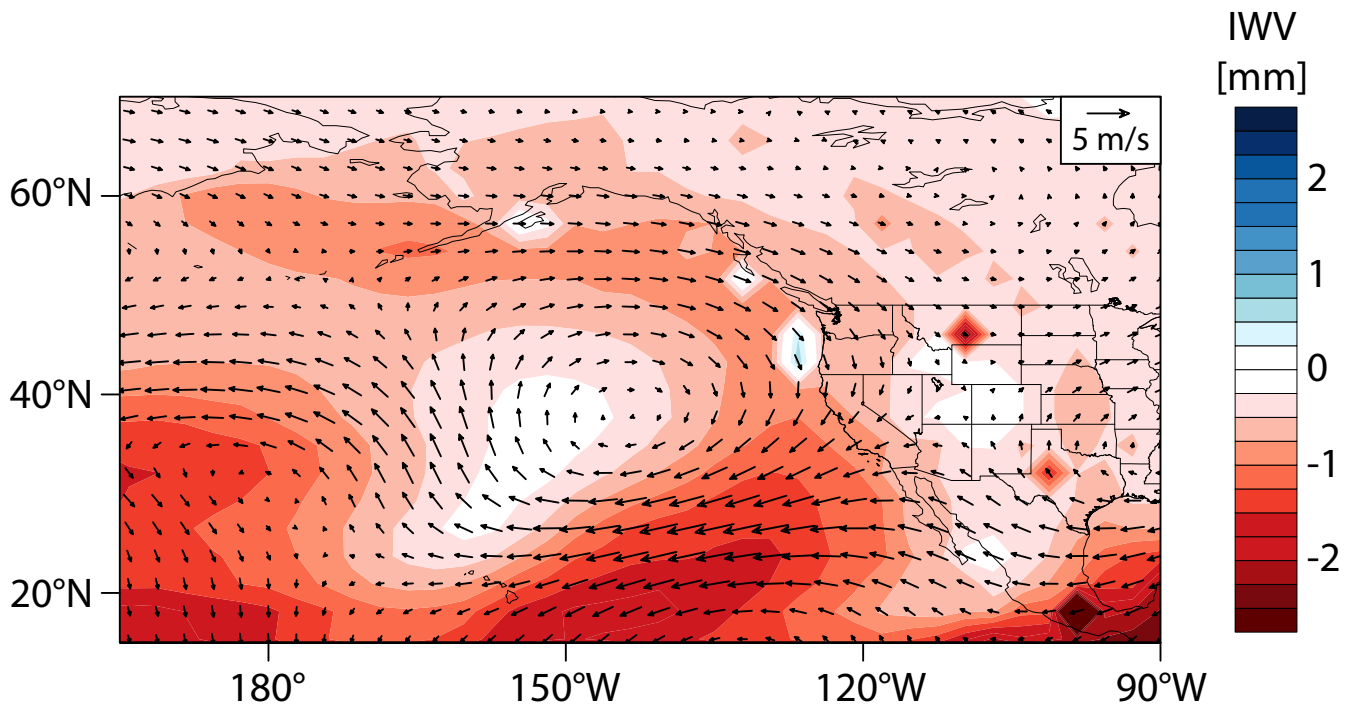


Figure 9. For FGOALS-g2, winter (DJF) mid-Holocene anomalies (6–0 ka) in integrated water vapor [IWV (mm) shading] and 250-hPa winds (vectors). IWV is calculated as the integral of water vapor (specific humidity) from the surface to the top of the atmosphere, for each grid cell (cf. Lora *et al.*, 2016).

transient upper level ridging that blocked and reduced moisture delivery to the continent during the cool season. This response is consistent with changes in moisture transport and meridional wind variability noted by models during the megadroughts of the Medieval Climate Anomaly and predicted by models for future global warming scenarios. Furthermore, the pattern of mid-Holocene drying over most of western North America with the exception of the south-west, as is seen in the annual and winter precipitation anomalies for FGOALS-g2, is consistent with the pattern of hydroclimatic change observed during CP El Niño events at the modern day, pointing to an area for future investigation with respect to western North American hydroclimate of the mid-Holocene.

Acknowledgements. We thank three anonymous reviewers for constructive comments on this work. This work was supported by NSF grants AGS-1203701 and AGS-1554998 to J.L.O. D.E.I. is supported by a Stanford EDGE-STEM fellowship. We thank Matthew Winnick, Jeremy Caves and Neil Kelley for help with analytical tools associated with this work. We thank the modeling groups for archiving results through the CMIP5 Data Portal (pcmdi9.llnl.gov/). All data used in model–proxy comparisons are available in the supporting information and are available for download from the NOAA National Climatic Data Center's Paleoclimatology database.

Supporting Information

Figure S1. PMIP3 modeled annual precipitation anomalies (6–0 ka).

Figure S2. PMIP3 modeled annual effective moisture anomalies (6–0 ka).

Figure S3. Precipitation KS test results for all mid-Holocene models for which monthly precipitation output was archived. Maps show regions determined to be wetter (blue) or drier (red) than the Pre-Industrial simulations at the 95% confidence level. Insignificant areas are mapped as no change (white). Precipitation fields were analyzed at the native model output resolution without contouring.

Figure S4. Same as Fig. S3 but for modeled mid-Holocene effective moisture.

Table S1. Mid-Holocene proxy network compiled for this analysis including information on record location, type of archives and proxies used, and references.

Table S2. Sites combined using a 25-km buffer radius. Bold sites are the aggregate locations, and italicized sites are the constituents.

Table S3. Proxy network used for calculation of Cohen's kappa, including aggregate sites.

Abbreviations. AL, Aleutian Low; CP, Central Pacific; EM, effective moisture; ENSO, El Niño/Southern Oscillation; EP, Eastern Pacific; ESGF, Earth System Grid Federation; IWV, integrated water vapor; KS, Kolmogorov–Smirnov; LGM, Last Glacial Maximum; NC, no change; NPH, North Pacific High.

References

- Adams DK, Comrie AC. 1997. The North American monsoon. *Bulletin of the American Meteorological Society* **78**: 2197–2213.
- An S-I, Choi J. 2014. Mid-Holocene tropical Pacific climate state, annual cycle, and ENSO in PMIP2 and PMIP3. *Climate Dynamics* **43**: 957–970.
- Bartlein PJ, Anderson KH, Anderson PM *et al.* 1998. Paleoclimate simulations for North America over the past 21,000 years: features of the simulated climate and comparisons with paleoenvironmental data. *Quaternary Science Reviews* **17**: 549–585.
- Bartlein PJ, Harrison SP, Brewer S *et al.* 2011. Pollen-based continental climate reconstructions at 6 and 21 ka: a global synthesis. *Climate Dynamics* **37**: 775–802.
- Bartoń K. 2014. MuMIn: multi-model inferences, R package. R Foundation for Statistical Computing. cran.r-project.org/web/packages/MuMIn/MuMIn.pdf.
- Bony S, Stevens B, Frierson DMW *et al.* 2015. Clouds, circulation and climate sensitivity. *Nature Geoscience* **8**: 261–268.
- Braconnot P, Harrison SP, Kageyama M *et al.* 2012. Evaluation of climate models using palaeoclimatic data. *Nature Climate Change* **2**: 417–424.

- Burnham KP, Anderson DR. 2002. *Model Selection and Multimodel Inference: a Practical Information-Theoretic Approach*, 2nd edn. Springer: New York.
- Delire C, Levis S, Bonan G, *et al.* 2002. Comparison of the climate simulated by the CCM3 coupled to two different land-surface models. *Climate Dynamics* **19**: 657–669.
- Chevalier M, Brewer S, Chase BM. 2017. Qualitative assessment of PMIP3 rainfall simulations across the eastern African monsoon domains during the mid-Holocene and Last Glacial Maximum. *Quaternary Science Reviews* **156**: 107–120.
- Coats S, Smerdon JE, Cook BI *et al.* 2016. Internal ocean-atmosphere variability drives megadroughts in Western North America. *Geophysical Research Letters* **43**: 9886–9894.
- Cohen J. 1968. Weighted kappa: nominal scale agreement with provision for scaled disagreement or partial credit. *Psychological Bulletin* **70**: 213–220.
- COHMAP Members. 1988. Climatic changes of the last 18,000 years: observations and model simulations. *Science* **241**: 1043–1052.
- Conroy JL, Overpeck JT, Cole JE *et al.* 2008. Holocene changes in eastern tropical Pacific climate inferred from a Galapagos lake sediment record. *Quaternary Science Reviews* **27**: 1166–1180.
- Dai A. 2006. Precipitation characteristics in eighteen coupled climate models. *Journal of Climate* **19**: 4605–4630.
- Dalmonech D, Zaehle S, Schürmann GJ *et al.* 2015. Separation of the effects of land and climate model errors on simulated contemporary land carbon cycle trends in the MPI earth system model version 1. *Journal of Climate* **28**: 272–291.
- Diffenbaugh NS, Sloan LC. 2004. Mid-Holocene orbital forcing of regional-scale climate: a case study of Western North America using a high-resolution RCM. *Journal of Climate* **17**: 2927–2937.
- Diffenbaugh NS, Sloan LC, Snyder MA *et al.* 2003. Vegetation sensitivity to global anthropogenic carbon dioxide emissions in a topographically complex region. *Global Biogeochemical Cycles* **17**. DOI: 10.1029/2002GB001974
- DiNezio PN, Tierney JE. 2013. The effect of sea level on glacial Indo-Pacific climate. *Nature Geoscience* **6**: 485–491.
- ESRI. 2014. *ArcGIS Desktop 10.2*. Environmental Systems Research Institute, Redlands.
- Fuentes-Franco R, Giorgi F, Coppola E *et al.* 2016. The role of ENSO and PDO in variability of winter precipitation over North America from twenty first century CMIP5 projections. *Climate Dynamics* **46**: 3259–3277.
- Garfinkel CI, Hurwitz MM, Waugh DW *et al.* 2013. Are the teleconnections of Central Pacific and eastern Pacific el Niño distinct in boreal wintertime? *Climate Dynamics* **41**: 1835–1852.
- Gavin DG, Brubaker LB. 2015. Late Pleistocene and Holocene environmental change on the Olympic Peninsula, Washington. In *Ecological Studies* 222. Springer: New York.
- Griggs C, Peteet D, Kromer B *et al.* 2017. A tree-ring chronology and paleoclimate record for the Younger Dryas-Early Holocene transition from northeastern North America. *Journal of Quaternary Science* **32**: 341–346.
- Harrison SP, Bartlein PJ, Brewer S *et al.* 2014. Climate model benchmarking with glacial and mid-Holocene climates. *Climate Dynamics* **43**: 671–688.
- Harrison SP, Bartlein PJ, Izumi K *et al.* 2015. Evaluation of CMIP5 palaeo-simulations to improve climate projections. *Nature Climate Change* **5**: 735–743.
- Harrison SP, Bartlein PJ, Prentice IC. 2016. What have we learnt from palaeoclimate simulations? *Journal of Quaternary Science* **31**: 363–385.
- Harrison SP, Kutzbach JE, Liu Z *et al.* 2003. Mid-Holocene climates of the Americas: a dynamical response to changed seasonality. *Climate Dynamics* **20**: 663–688.
- Hatchett BJ, Boyle DP, Garner CB *et al.* 2016. Magnitude and frequency of wet years under a megadrought climate in the western Great Basin, USA. *Quaternary Science Reviews* **152**: 197–202.
- Higgins RW, Shi W. 2005. Relationships between Gulf of California Moisture Surges and Tropical Cyclones in the Eastern Pacific Basin. *Journal of Climate* **18**: 4601–4620.
- Horton DE, Johnson NC, Singh D *et al.* 2015. Contribution of changes in atmospheric circulation patterns to extreme temperature trends; 1; *Nature* **522**: 465–469.
- Kanamitsu M, Ebisuzaki W, Woollen J *et al.* 2002. NCEP–DOE AMIP-II Reanalysis [R-2]. *Bulletin of the American Meteorological Society* **83**: 1631–1643.
- Karamperidou C, Di Nezio PN, Timmermann A *et al.* 2015. The response of ENSO flavors to mid-Holocene climate: implications for proxy interpretation. *Paleoceanography* **30**: 527–547.
- Koutavas A, deMenocal PB, Olive GC *et al.* 2006. Mid-Holocene El Niño-Southern Oscillation (ENSO) attenuation revealed by individual foraminifera in eastern tropical Pacific sediments. *Geology* **34**: 993–996.
- Koutoulis AG, Grillakis MG, Tsanis IK *et al.* 2016. Evaluation of precipitation and temperature simulation performance of the CMIP3 and CMIP5 historical experiments. *Climate Dynamics* **47**: 1881–1898.
- Lora JM, Mitchell JL, Risi C *et al.* 2017. North Pacific atmospheric rivers and their influence on western North America at the Last Glacial Maximum. *Geophysical Research Letters* **44**: 1051–1059.
- Lora JM, Mitchell JL, Tripathi AE. 2016. Abrupt reorganization of north Pacific and western North American climate during the last deglaciation. *Geophysical Research Letters* **43**: 11,796–11,804.
- Massey, Jr FJ. 1951. The Kolmogorov-Smirnov test for goodness of fit. *Journal of the American Statistical Association* **46**: 68–78.
- Mejia JF, Douglas MW, Lamb PJ. 2016. Observational investigation of relationships between moisture surges and mesoscale- to large-scale convection during the North American Monsoon. *International Journal of Climatology* **36**: 2555–2569.
- Metcalf SE, Barron JA, Davies SJ. 2015. The Holocene history of the North American Monsoon: ‘known knowns’ and ‘known unknowns’ in understanding its spatial and temporal complexity. *Quaternary Science Reviews* **120**: 1–27.
- Mock CJ, Brunelle-Daines AR. 1999. A modern analogue of western United States summer palaeoclimate at 6000 years before present. *Holocene* **9**: 541–545.
- Moy CM, Seltzer GO, Rodbell DT *et al.* 2002. Variability of el Niño/Southern Oscillation activity at millennial timescales during the Holocene epoch. *Nature* **420**: 162–165.
- Myers CG, Oster JL, Sharp WD *et al.* 2015. Northeast Indian stalagmite records Pacific decadal climate change: implications for moisture transport and drought in India. *Geophysical Research Letters* **42**: 4124–4132.
- Nederbragt AJ, Thurow J. 2005. Amplitude of ENSO cycles in the Santa Barbara Basin, off California, during the past 15000 years. *Journal of Quaternary Science* **20**: 447–456.
- NOAA. 2008. ETOPO1 Arc-Minute Global Relief Model. NOAA: Silver Spring.
- Oster JL, Ibarra DE, Winnick MJ *et al.* 2015. Steering of westerly storms over western North America at the Last Glacial Maximum. *Nature Geoscience* **8**: 201–205.
- Oster JL, Kelley NP. 2016. Tracking regional and global teleconnections recorded by western North American speleothem records. *Quaternary Science Reviews* **149**: 18–33.
- Parker LE, Abatzoglou JT. 2016. Spatial coherence of extreme precipitation events in the Northwestern United States. *International Journal of Climatology* **36**: 2451–2460.
- Seager R, Burgman R, Kushnir Y *et al.* 2008. Tropical Pacific forcing of North American Medieval megadroughts: testing the concept with an atmosphere model forced by coral-reconstructed SSTs. *Journal of Climate* **21**: 6175–6190.
- Shuman BN, Serravezza M. 2017. Patterns of hydroclimatic change in the Rocky Mountains and surrounding regions since the last glacial maximum. *Quaternary Science Reviews* **173**: 58–77.
- Simpson IR, Seager R, Ting M *et al.* 2016. Causes of change in Northern Hemisphere winter meridional winds and regional hydroclimate. *Nature Climate Change* **6**: 65–70.
- PAGES 2k Consortium. 2013. Continental-scale temperature variability during the past two millennia. *Nature Geoscience* **6**: 339–346.
- Taylor KE, Stouffer RJ, Meehl GA. 2012. An overview of CMIP5 and the experiment design. *Bulletin of the American Meteorological Society* **93**: 485–498.

- Thompson RS, Anderson KH. 2000. Biomes of western North America at 18,000, 6000 and 0 14C yr bp reconstructed from pollen and packrat midden data. *Journal of Biogeography* **27**: 555–584
- Thompson RS, Whitlock C, Bartlein PJ *et al.* 1993. Climatic Changes in the Western United States since 18,000 yr B.P. In *Global Climates Since the Last Glacial Maximum*, Wright HE, Kutzbachm JE, Webb T, III, Ruddiman WF, Street-Perrott FA, Bartlein PJ (eds). University of Minnesota Press, Minneapolis; 468–513.
- Trenberth KE. 2011. Changes in precipitation with climate change. *Climate Research* **47**: 123–138.
- Weng H, Behera SK, Yamagata T. 2009. Anomalous winter climate conditions in the Pacific Rim during recent el Niño Modoki and El Niño events. *Climate Dynamics* **32**: 663–674.
- Wise EK. 2010. Spatiotemporal variability of the precipitation dipole transition zone in the western United States. *Geophysical Research Letters* **37**: L07706.
- Wise EK. 2016. Five centuries of US West Coast drought: occurrence, spatial distribution, and associated atmospheric circulation patterns. *Geophysical Research Letters* **43**: 4539–4546.
- Zheng W, Braconnot P, Guilyardi E *et al.* 2008. ENSO at 6ka and 21ka from ocean–atmosphere coupled model simulations. *Climate Dynamics* **30**: 745–762.